Proton Emission in 42-MeV Alpha-Particle Bombardments of Several Elements*

R. W. WEST†
University of Washington, Seattle, Washington
(Received 9 August 1965)

Measurements have been made of the energy spectra, angular distributions, and absolute cross sections of protons emitted from bombardments of Co^{59}, Ni^{58}, Ni^{60}, $^{e}Ni^{62}$, Cu^{63}, Cu^{65}, Nb, Rh, Pd, and Pt targets by 42-MeV alpha particles. A dE/dX-E scintillation telescope was used in conjunction with an x, y oscilloscope to detect and identify protons in the energy range from 2 to 40 MeV. The data were compared with predictions of the statistical model of nuclear reactions. A calculation was made of the expected proton energy spectra based on this model. The cascade was restricted to neutron and proton emission only, and a level density of the form $\{\exp 2[a(U-\delta)]^{1/2}\}/(U-\delta)^2$ was used. Except for Pt, the calculated and experimental energy spectra matched in slope over a relatively wide intermediate-energy region with the observed spectrum, exceeding the calculated spectrum in both the lowest and highest energy regions. The lowest energy protons were assumed to be caused by compound-nuclear events and the data were separated into compound-nuclear and non-compound-nuclear portions. It was found that the compound-nuclear portions agree well with expectations of the statistical model for yields, spectra, and angular distributions, and they account for 90% of the proton yield for targets in the Ni region, 65% of the proton yield for targets in the Rh region, and probably less than 6% of the proton yield for Pt. The non-compound-nuclear component exhibits a relatively constant yield of ≈ 85 mb for all the targets studied.

I. INTRODUCTION

IN bombardments at a few tens of MeV, it seems clear that most of the interactions give rise to a compound nucleus which subsequently de-excites by the statistical evaporation of particles.[1,2]

One is led to this conclusion by an examination of the yields and distributions of emitted particles. For example, the excitation functions for specific reactions [e.g., $(\alpha,2np)$] rise sharply soon after their threshold to a maximum which is an appreciable fraction of the total reaction cross section. Then they fall off fairly rapidly when the threshold for the next higher important reaction is passed.[2] The particle emission spectra tend to have low mean energies and a more or less classical Maxwellian character.[3–5] The yields of particles with large binding energies or which have high Coulomb barriers to surmount are depressed.[6,7] The angular distributions and correlations between emitted particles show symmetries characteristic of a long lifetime and statistical emission.[8–10]

Indeed generally the qualitative agreement between the observations and expectations based on a statistical picture of the particle emission has been good enough to encourage the refinement of the statistical models and attempts to extract from the observations the important parameters of such models.[2,11] Such parameters include, for example, effective Coulomb barrier heights, inverse nuclear cross sections for emitted particles, and the parameter a appearing in the exponent of the commonly used expression for the nuclear level density. One has tried to learn how these parameters vary with nuclear species (i.e., with Z and A) as well as with excitation energy.[2,12–14]

The extraction of these parameters in a reliable way has proved to be more difficult than one had perhaps anticipated. The difficulties arise from essentially two sources. (1) The spectra and distributions that one observes result from emissions at a variety of excitation energies, and comparisons between observation and expectation generally involve the (often uncertain) superposition of a number of computed distributions. (2) Almost from the outset it has been clear that not *all* of the particles are evaporated, but that some (perhaps of the order of 10%) tend to come out with more than average energy, generally in the forward direction. These are presumbaly direct products of the initial interaction of the incident projectile with the nucleus. Although these so-called direct particles are relatively few, they tend to dominate the high-energy parts of the spectrum, where measurements are relatively easier to make, and they can easily confound the usual analysis. For example, studies of emission spectra have been interpreted as showing that the nuclear level-density parameter a, tends to remain independent of A although general statistical considerations would have it be proportional to A.[15–17] Although it seems reasonable that

* Supported in part by U. S. Atomic Energy Commission.
† Now at the University of Rochester, Rochester, New York.
[1] D. Bodansky, Ann. Rev. Nucl. Sci. **12**, 79 (1962).
[2] I. Dostrovsky, Z. Fraenkel, and G. Friedlander, Phys. Rev. **116**, 683 (1959), referred to as D.F.F.
[3] D. Drake, Ph.D. thesis, University of Washington, 1962 (unpublished).
[4] R. Sherr and F. P. Brady, Phys. Rev. **124**, 1928 (1961).
[5] R. M. Eisberg and G. Igo, Phys. Rev. **93**, 1039 (1954).
[6] E. F. Neuzil and R. H. Lindsay, Phys. Rev. **131**, 1697 (1963).
[7] G. Merkel, University of California Radiation Laboratory Report No. UCRL-9898, 1961 (unpublished).
[8] C. Gruhn, Ph.D. thesis, University of Washington, 1961 (unpublished).
[9] D. Bodansky, R. K. Cole, W. G. Cross, C. R. Gruhn, and I. Halpern, Phys. Rev. **126**, 1082 (1962).
[10] N. Lassen and V. Siderov, Nucl. Phys. **19**, 579 (1960).
[11] D. W. Lang, Nucl. Phys. **26**, 434 (1961).
[12] G. Igo and B. D. Wilkins, University of California Radiation Laboratory Report No. UCRL-10568, 1962 (unpublished).
[13] G. Igo and B. D. Wilkins, Phys. Rev. **129**, 2198 (1963).
[14] M. Blann and G. Merkel, Nucl. Phys. **52**, 673 (1964).
[15] R. M. Eisberg, G. Igo, and H. E. Wegner, Phys. Rev. **100**, 1309 (1955).
[16] J. B. Mead and B. L. Cohen, Phys. Rev. **125**, 947 (1962).
[17] W. Swenson and C. Gruhn, Bull. Am. Phys. Soc. **8**, 357 (1963).

the apparent constancy of a may be attributable to the (relatively A-independent) contribution of direct emissions to observed spectra, it is difficult to establish such a point in the absence of a consistent way to distinguish evaporated from directly emitted particles.

The present study of proton emission in 42-MeV alpha-particle bombardments of a variety of nuclei was undertaken to examine more closely the spectra and distributions of emitted particles.[18] The main goal was to see if one could in a meaningful and consistent way divide the observations into direct and evaporated particles where the latter have the expected properties and the former behave smoothly as a function of nuclear species and bombarding energy.

To this end, the spectra were measured carefully over a broad energy range extending from ≈ 2 MeV (which is well below the energies generally examined) to the highest emission energies (over 25 MeV). The angular distributions were also examined over a broad range (from 30° to 150°). To help with the identification of the two emission components, a calculation was carried out of the expected evaporation spectrum for each observed situation, (Sec. IV). The calculation was kept simple in structure and used what seem to be the most reasonable values of nuclear parameters available. It is found to give a good (but not spectacular) account of the lower energy parts of the observed spectra. It is used as the basis for a subtraction of the evaporation component from the observations, permitting the extraction of a direct component. The paper concludes with an examination of the amount, spectrum, and angular distribution of this important but hitherto poorly characterized component of the emission spectrum in medium-energy reactions.

II. EXPERIMENTAL METHOD

The University of Washington 60-in. cyclotron produces beams of 10.5-MeV protons, 21-MeV deuterons or 42-MeV alpha particles. A system of magnets provides some momentum selection and directs the beam into a 60-in. scattering chamber.[19] The scattering chamber contains a beam collimator, two movable detector arms and a target holder and changer. A Faraday cup is attached to the far end of the chamber. A target beam spot approximately $\frac{1}{16}$ in. wide and $\frac{3}{8}$ in. high was defined by graphite slits held in a water-cooled aluminum collimation tube.

The targets used, together with their purity, thickness, and the source from which they were obtained are listed in Table I. A check of the uniformity of the targets was made through the use of a thickness gauge consisting of a solid-state detector viewing an alpha-particle source through the target. Variations in thickness of less than 1% (for a target approximately 3 mg/cm² thick) could be detected.

TABLE I. Targets.

Target	Thickness (mg/cm²)	Isotopic purity	Major impurity
Co^{59} [a]	2.87±0.06	Natural	Unknown
Ni^{58} [b]	3.16±0.22	99.1%	0.76% Ni^{60}
Ni^{60} [b]	2.64±0.30	99.0%	0.30% Ni^{58}
Ni^{62} [a]	3.29±0.23	97.96%	1.09% Ni^{60}
Cu^{63} [b]	2.10[d]	99.76%	0.24% Cu^{65}
Cu^{65} [b]	1.86±0.09	99.40%	0.60% Cu^{63}
Nb[c]	13.30±0.20	Natural	Unknown
Rh[c]	9.12±0.18	Natural	Unknown
Pd[c]	10.58±0.20	Natural	Unknown
Pt[c]	5.81±0.12	Natural	Unknown

[a] Target obtained from Oak Ridge National Laboratory, Isotope Division, Oak Ridge, Tennessee.
[b] Target obtained from Harwell, Atomic Energy Research Establishment.
[c] Target obtained from University of Washington Cyclotron target file.
[d] Target thickness given is believed to be within 30% of true thickness which was not determinable (see discussion).

A survey of the surface of the naturally occuring targets used (Co^{59}, Nb, Rh, and Pd) showed them to be uniform to within 2%. The absolute thickness of these targets and the Pt (the Pt target was assumed uniform) was therefore found by direct measurement of their weight and area. The Cu^{65} target was somewhat less uniform and the consequent uncertainty in its thickness was 5%.

Both the Cu^{63} and Ni targets showed considerable variations in thickness. A detailed survey of the Cu^{63} target was not possible because this target was accidentally shattered by a vacuum leak. Thus the Cu^{63} data are included only for the shapes of the energy spectra and angular distributions. The relative thicknesses of the Ni isotope targets were found by a comparison of counting rates for what was assumed to be Rutherford scattered protons at a laboratory angle of 10°. The data of Hintz[20] and the analysis by Glassgold *et al.*[21] of elastic proton scattering from Ni at 9.8 MeV indicate this assumption could be in error by as much as 5%. However, deviations from Rutherford scattering should be approximately the same for Ni^{58}, Ni^{60}, and Ni^{62}.[22] Relative errors in the target thicknesses of the Ni^{58}, Ni^{60}, and Ni^{62} are estimated to be 3, 10, and 3%, respectively. The Ni^{60} target was particularly nonuniform, as reflected in the higher assigned error. For this reason, the complete angular distribution from Ni^{60} was measured without changing the position of this target in the target changer-holder. (Fortunately, a hydrogen contaminant on the target made it possible to check the energy calibration stability at forward angles.) The absolute thickness of the Ni targets listed in Table I is based on a Rutherford-scattering comparison with a natural Ni target of known thickness.

The beam passing through the target was collected

[18] A more detailed description of this work is given by R. W. West, Ph.D. thesis, University of Washington, 1963 (unpublished).
[19] University of Washington Cyclotron Research, 1957 (unpublished).
[20] N. M. Hintz, Phys. Rev. **106**, 1201 (1957).
[21] R. E. Glassgold, W. B. Cheston, M. L. Stein, S. B. Schuldt, and G. M. Erickson, Phys. Rev. **106**, 1207 (1957).
[22] See, for example, J. Benveniste, R. Booth, and A. Mitchell, Phys. Rev. **123**, 1818 (1961).

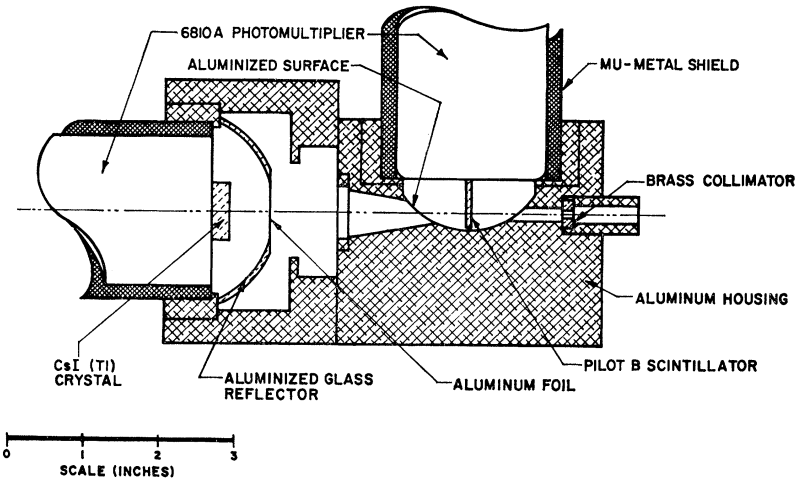

FIG. 1. Vertical section of the proton detector.

in a Faraday cup consisting of a 6-in.-diam, 16-in.-long aluminum cylinder backed by a graphite catcher disk. The disk was located approximately 60 in. from the target. The charge accumulated in the Faraday cup was stored in a precision polystyrene capacitor and read upon discharge on a ballistic galvanometer. Because back scattering of electrons and ionization by the beam of residual gas in the vicinity of the cup can produce measurable effects, the absolute value of the charge collected is in doubt. Recent measurements[23] of elastic cross sections at forward angles using a biased Faraday cup have shown agreement to within 5% with calculated Rutherford-scattering cross sections. Allowing for uncertainties in the measurements, it is concluded that the absolute values of the Faraday-cup readings were not in error by more than 10%. It is believed that the relative measurements are correct to within 5%.

The detection of protons from 2 to 40 MeV was accomplished by a dE/dx-E scintillation telescope using two RCA 6810-A photomultipliers mounted in separate aluminum housings, (see Fig. 1). The telescope's aperature consisted of a 0.125 ± 0.002-in. circular collimator placed 7.00 ± 0.03 in. from the target.

The E scintillator, a 1-in.-diam, $\frac{1}{4}$-in.-thick CsI(Tl) crystal, was coupled directly to its phototube with Dow Corning C-2-0057 fluid. An aluminized curved section of glass acted as reflector. This arrangement typically gave 4% full width at half-maximum (FWHM), for 10-MeV protons.

The use of a 0.002-in. sheet of plastic Pilot B scintillator as the dE/dx crystal together with a thin aluminum (1/20 mil) light shield placed between the two crystals gave a counter threshold of 2 MeV. This low threshold was necessary because of the importance of low-energy protons in the emission spectrum for the targets near $Z=30$.

The resolution (28% for 10-MeV protons) resulting from the use of this thin plastic was insufficient to distinguish deuterons from protons (see Fig. 2). Although increasing the thickness to 0.010 in. produced adequate separation between deuterons and protons, it raised the detector threshold to approximately 5 MeV. As a result, proton spectra were collected in two parts. The first part, with a 0.002-in. dE/dx detector, contained protons and deuterons in the 2- to 20-MeV range, while the second part contained only protons and extended from 5 to 40 MeV. This composite spectrum is believed to be essentially free of deuteron contamination even below 5 MeV. A typical case illustrated by Fig. 3 shows a constant or decreasing density of deuterons from high to low energy while the density of protons strongly increases in this region. The contention that there are few low-energy deuterons is further supported by the excellent overlap of the 2- and 10-mil spectra at 6 MeV shown in Fig. 4. The deuteron contamination of the proton spectra below 5 MeV is estimated to be less than 0.5%. Because of their greater stopping power, tritons,

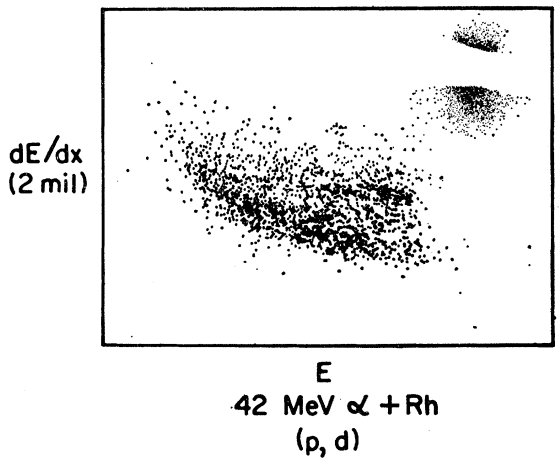

FIG. 2. Dot plot (dE/dx versus E) of unresolved protons and deuterons using the 2-mil plastic dE/dx scintillator. Elastic alpha particles appear as a faint glow behind mask in the upper-right-hand corner.

[23] Isam Naqib, Ph.D. thesis, University of Washington, 1962 (unpublished).

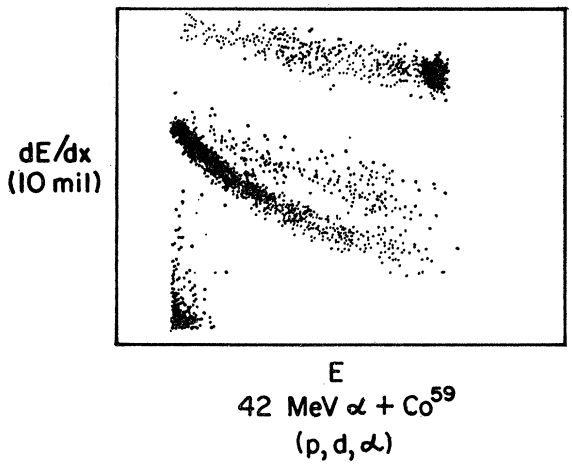

FIG. 3. Dot plot (dE/dx versus E) of alpha particles, deuterons, and protons, using the 10-mil plastic dE/dx scintillator. The protons form the lower band. A partially resolved excited state can be seen in the alpha-particle band. The spots at the lower left and extending up the dE/dx axis are caused by background events. The counter was at 30°.

He^3, and He^4 particles were easily separated from protons.

Electrical pulses produced in both the dE/dx and E counters by reaction products from the target were fed first to preamplifiers and then to the counting-room area located approximately 100 ft from the scattering chamber. As shown in Fig. 5, the E pulse passed through a delay line used for timing purposes and then to the internal linear amplifier of a 512-channel analyzer (Nuclear Data Model ND 120). The analyzer was "gated on" by the output of the particle identification system. Data for successive runs were collected separately in each of four 128-channel quadrants before being read out on paper tape and finally to a typewriter.

Particle identification was accomplished through the use of an x, y oscilloscope system[24] which displayed the functional relationship between dE/dx and E.

Calibration of the energy spectra from 2 to 22 MeV was accomplished through the use of protons resulting from elastic collisions between 42-MeV beam α particles and the hydrogen of a polyethylene target. The $C^{12}(\alpha,p)N^{15}$ reaction was used to obtain a higher energy proton calibration point (32.2 MeV at 30°). In order to compensate for differences in target energy loss between the calibration polyethylene target and the targets used in the experiment, special care was taken to match each target with a polyethylene target of equivalent energy thickness for low-energy protons. Furthermore, a constant angle of 45° was maintained between the proton counter and the target for all data and calibration runs.

The accuracy of this calibration procedure is limited by uncertainties in the counter angle and in the beam energy. The counter angle was known to better than 0.1° which is equivalent to 47 keV at an angle of 45°. The deviation of the true beam energy from 42.0 MeV is estimated to be less than 200 keV. No corrections were made for incident α-particle energy losses in the target. This is reasonable for the Co, Ni, and Cu targets, because, on the average, these targets degraded the beam by less than $\frac{1}{2}\%$ of its full energy. In the worst case, 13.3 mg/cm^2 of Nb, the energy correction would be 1.4% or 140 keV for a 10-MeV proton.

During a typical run, an energy check was made after collection of data at three angles with a complete calibration after every six angles. These checks were supplemented in some instances by the self-calibration of a target because of the presence of a hydrogen contaminant. This recoil proton peak in forward angle data served as both an energy calibration point and a stability check of the electronics.

The efficiency of the proton detecting system as a function of proton energy was measured for each series of runs in which the 2-mil dE/dx crystal was used. The system was found to detect virtually all protons at all energies except at threshold where the efficiency decreased suddenly and rapidly. Thus the measurement was not used to correct the raw data, but served only to indicate the lower energy limit of reliable data.

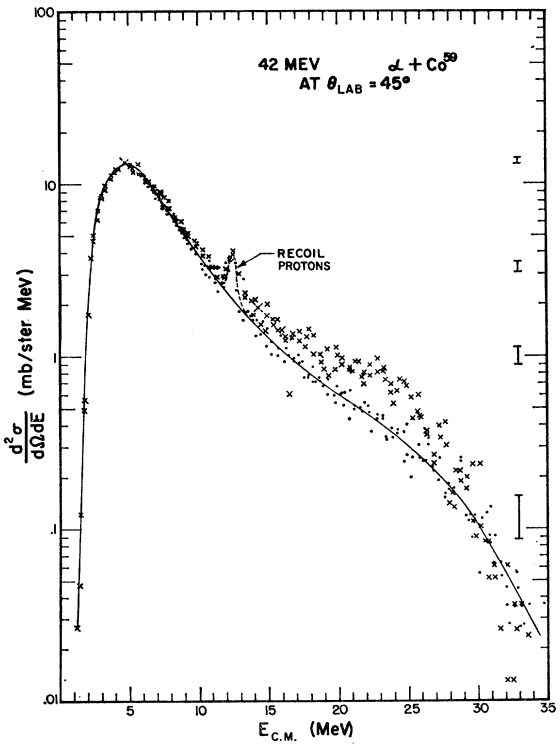

FIG. 4. Center-of-mass energy spectrum for Co^{59}. Two sets of data denoted by crosses and dots have been superimposed on an absolute scale. The crosses denote data collected with the 2-mil dE/dx scintillator and dots denote data collected with the 10-mil dE/dx scintillation. Deuterons in the 2-mil data at high energies cause the two sets of points to separate. The solid line indicates the proton yield only. The recoil peak at about 12 MeV is presumed to be due to a thin surface hydrocarbon film.

[24] University of Washington Cyclotron Research, 1962 (unpublished).

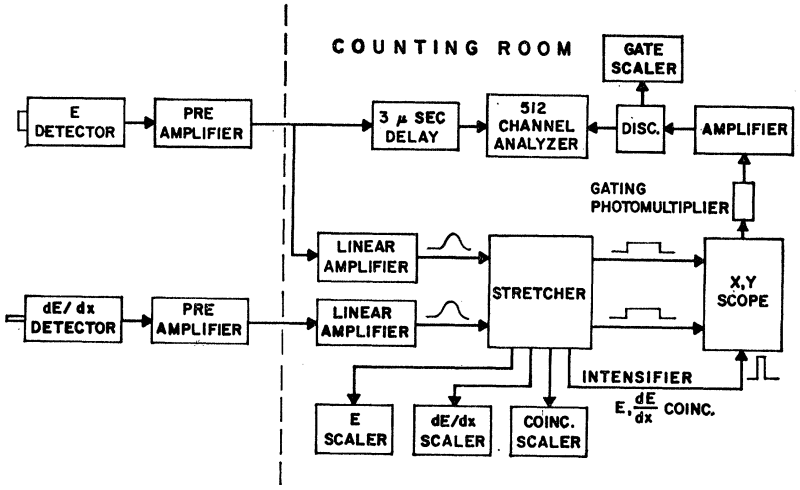

FIG. 5. Block diagram of electronics.

The efficiency measurement at low energies involved the use of two detectors: the proton counter described above, and a second scintillator detector placed 90° to it on the opposite side of the beam. Protons produced by elastically scattering the 10.5-MeV proton beam from hydrogen in a polyethylene target were detected in coincidence by the dE/dx crystal of the proton counter and this second scintillation detector. This double coincidence gated the second detector's spectrum displayed on a 20-channel analyzer. By adding the requirement that a proton be detected in the E portion of the dE/dx-E counter, a triple coincidence was formed which gated the E signal displayed in the 512-channel analyzer. The efficiency was then the ratio of the E pulses recorded in the 512-channel analyzer to the second detector's pulses recorded in the 20-channel analyzer. This somewhat complicated system was used to reject coincidence events (including accidental coincidences) which had an incorrect energy for elastic p-p scattering. By varying the angle of the detectors, relative to the beam, the efficiency as a function of energy was measured from threshold to 7 MeV. This technique measured the efficiency for the entire detecting system from detector to analyzer and showed the system to be virtually 100% efficient for low-energy protons above an energy of 2.8 MeV. Below this energy, the efficiency decreased to 50% at 2.3 MeV with the threshold occurring at about 2.0 MeV.

The system was assumed to be 100% efficient above 7 MeV where the coincident measurement could not be used. The higher energy protons lose less energy in the dE/dx portion of the detector and above some energy this loss will be below the dE/dx detection threshold. Photographs of the x, y scope (such as seen in Fig. 2) indicated that protons as high as 30 MeV were safely above this threshold even with the 2-mil dE/dx crystal in place. This was checked at 32 MeV by a measurement of the $C^{12}(\alpha,p)N^{15}$ reaction leading to the ground state of N^{15}. This measurement, when compared to that of Lieber, Schmidt, and Gerhart,[25] was found to agree within the experimental accuracy of 10%. This agreement at 32 MeV coupled with the fact that the high-energy portion of the proton spectra were recorded with the 10-mil crystal in place (which effectively lowered the dE/dx threshold) made it highly unlikely that any high-energy protons went undetected.

The existence of light target contaminants can be especially troublesome in the aspect of this experiment which is concerned with estimating direct interaction yields. The combination of a relatively large center-of-mass motion and the large direct-interaction cross sections results in extensive forward peaking of protons from carbon, nitrogen and oxygen. Previous experiments at this laboratory[8,26] have shown carbon, most likely from pump-oil hydrocarbons, to be the most abundant target contaminant. Further evidence for a build up of hydrocarbons on the surface of targets is given by the fact that the recoil proton peak exhibited by most of the forward angle spectra was not present in spectra obtained when these same targets were new. As a result of the methods described below, contaminants were found to be small, and it was decided to treat all the data as if no contamination were present.

An investigation of the amount of proton contamination caused by carbon for the Co^{59}, Ni^{60}, Ni^{62}, Cu^{65}, Nb, Rh, Pd, and Pt spectra was made through the combination of two measurements. First, the carbon content of the targets was measured by a comparison of the number of recoil carbon atoms in coincidence with elastically scattered alpha particles for these targets and for a polyethylene target (CH_2) of known thickness. (This measurement gave only an "upper limit" to the carbon content of the targets due to the unfortunate use of an excessively thick CH_2 target causing an underestimate of the carbon content of the cali-

[25] A. J. Lieber, F. H. Schmidt, and J. B. Gerhart, Phys. Rev. 126, 1496 (1962).
[26] C. Zafiratos, Ph.D. thesis, University of Washington, 1962 (unpublished).

bration target.) This gave an effective carbon thickness to normalize the second measurement, namely, the angular distribution of the proton spectra produced by the alpha-particle bombardment of carbon (polyethylene). A counter telescope consisting of a proportional gas dE/dx counter containing a junction E detector[27] was used in conjunction with the (x,y) oscilloscope system to detect and identify the recoil carbon nuclei. This detector was capable of identifying recoils ranging in mass from helium to fluorine and it therefore gave a measure of other contaminants relative to carbon. The results of these measurements showed the following:

(a) Carbon was the most abundant contaminant, contributing about 85% of the recoil products. Almost all of the remaining 15% was caused by oxygen.

(b) The amount of carbon present was about the same for all targets.

(c) Contaminants were concentrated on the surfaces of the targets as evidenced by the appearance of two distinct groups in the recoil spectra; the second group being degraded in energy by an amount equal to its energy loss in the target.

(d) Up to the point at which the reaction Q value terminated the carbon spectrum, the relative contamination was about the same for all energies with a slightly higher relative contribution at the lowest and highest energies.

(e) The over-all contamination caused by carbon in all but the Cu^{65}, Ni^{62}, and Pt spectra was less than 1% at forward angles and less than 0.2% at backward angles. [Because of (e) and (b), no measurement was made for Ni^{58} and Cu^{63} which were among the most proficient proton emitters.]

(f) The Cu^{65}, Ni^{62}, and Pt targets have less than a 7% contamination from carbon. This upper limit is thought to be considerably higher than the true amount of contamination because the characteristic peak structure of the carbon and oxygen spectrum was never visible in the primary spectrum. Taking the recoil proton peak to represent the hydrogen component of the contaminant with a $(CH)_n$ composition, the true contamination for these three targets would be close to 2.5% at forward angles and much less at backward angles. As a result of these considerations, it was decided to treat all the data as if no contamination was present. Although some contamination does exist in the energy spectra it certainly does not appreciably contribute to the spectrum at any energy and is considered to be sufficiently small at all angles and for all targets so as not to affect the final results or conclusions.

A rough measurement of the proton content of the alpha beam was made, which excluded such protons as a possible cause of the observed forward peaking of the proton angular distributions. Even a small number of protons in the primary alpha beam, possibly a result of slit scattering, could simulate a sizable direct-interaction spectrum, because the proton elastic scattering cross sections in medium and heavy nuclei are large at forward angles.

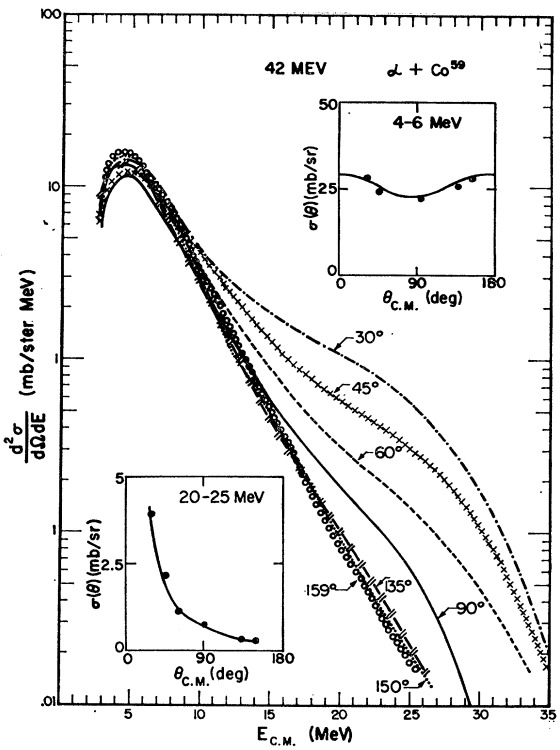

FIG. 6. Composite energy spectra for Co^{59}. The insets show the angular distributions of a low-energy group and a high-energy group of protons.

The measurement consisted of three parts. First, coincident protons originating from a polystyrene $(CH)_m$ target under alpha-particle bombardment, were detected at 45° to the beam. Second, the measurement was repeated using the 10.5-MeV proton beam, and third, a measurement of the elastic-scattering cross section of 10.5-MeV protons from Co^{59} was made at 45°. The first two measurements were designed to give the 10.5-MeV proton content of the alpha beam while the third gave the resulting contribution to the Co^{59} proton spectrum at 45°. The results set an upper limit of 3% on the part of the proton yield at 10 MeV from Co^{59} at 45° that could be due to the existence of a proton contamination in the alpha-particle beam. Thus the alpha beam contained insufficient proton contamination to account for the observed forward peaking of the Co^{59} data. This conclusion has been extended to include the observed spectra from all targets on the basis of the following arguments: (a) As discussed later, the observed high-energy protons are essentially independent of the target. This is true for both the spectral shapes and yields, and is therefore in conflict with the Z^2 dependence of Coulomb scattering. (b) The similarity of high-energy spectra implies a common mechanism in all tar-

[27] We are indebted to C. Zafiratos for the use of this detector (Ref. 26).

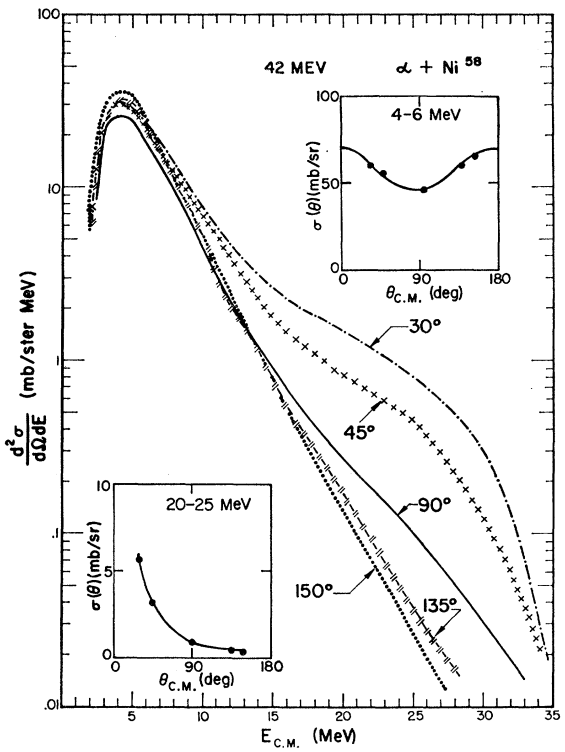

FIG. 7. Composite energy spectra for Ni^{58}. The insets show the angular distributions of a low-energy group and a high-energy group of protons.

gets; the experimental result for Co^{59} therefore indicates that this mechanism is not proton-beam contamination. (c) For two of the targets (Co^{59} and Rh), data were collected at 10°, 15° and 20°, and these data did not show a $\csc^4(\frac{1}{2}\theta)$ dependence required for Coulomb scattering. (For example, Coulomb scattering between 20° and 10° would increase at a rate 10 times that observed for Rh at 20 MeV.)

In a typical run, the raw data in the form of the number of counts per channel in the multichannel analyzer were read out on Tally punch paper tape and transferred to IBM tab cards by an IBM 836 tape-to-card unit. These cards, together with an energy calibration and a parameter card (containing the necessary masses and angles along with charge, solid-angle, and target-thickness data), formed the data deck for an IBM 709 computer code. This code was written for the specific purpose of transforming continuous spectra (as opposed to discrete levels) to the center-of-mass system, with normalization to give cross sections in millibarns per steradian per MeV. Prior to transforming the data, the code makes a least-squares fit of the laboratory energy calibration data to an equation of the form $y=aE-b/E+c$ where y is observed pulse height (channel number), a, b, and c are adjustable parameters, and E is the laboratory energy. It then finds the energy width of each channel from the slope of the energy calibration curve and finally produces the desired center-of-mass cross section $d^2\sigma/d\Omega dE$, using the transformation factor given by $(E_c/E_l)^{1/2}$. The subscripts c and l refer to energies in the center of mass and laboratory, respectively.

III. EXPERIMENTAL RESULTS

Figure 4 shows a typical experimental spectrum in the center-of-mass system. Similar spectra were obtained for other targets, in general at 30°, 45°, 90°, 135°, 150°, and 159°. Additional data was collected at 10°, 15°, 20°, 60°, and 120° for Co^{59} and Rh. (A degrader to exclude elastically scattered alpha particles was used for the 10°, 15° and 20° data. This raised the proton energy threshold from about 5 to 12 MeV.) Most of the forward-angle data contains a recoil-proton peak presumably from a thin hydrocarbon film on the target. This peak is illustrated by a dashed line in Fig. 4.

It should be noted that Fig. 4 is not a "true" center-of-mass spectrum at a single center-of-mass angle. This is because of the energy dependence of the correction between laboratory and center-of-mass angles. For example, for 5-MeV protons emitted from Ni^{60}, 30° in the laboratory corresponds to 32.7° in the center of mass, and 90° in the laboratory corresponds to 95° in the center of mass. Fortunately, where the corrections are largest (low energies at 90°), the cross-sectional variation with angle is small, and at high energies where the total yield changes most rapidly with angle, the corrections are small. As a result, the distortions of these

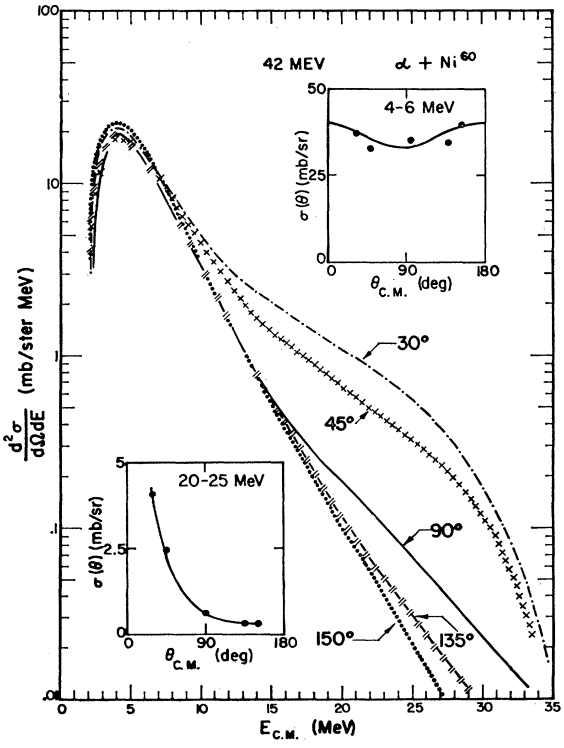

FIG. 8. Composite energy spectra for Ni^{60}. The insets show the angular distributions of a low-energy group and a high-energy group of protons.

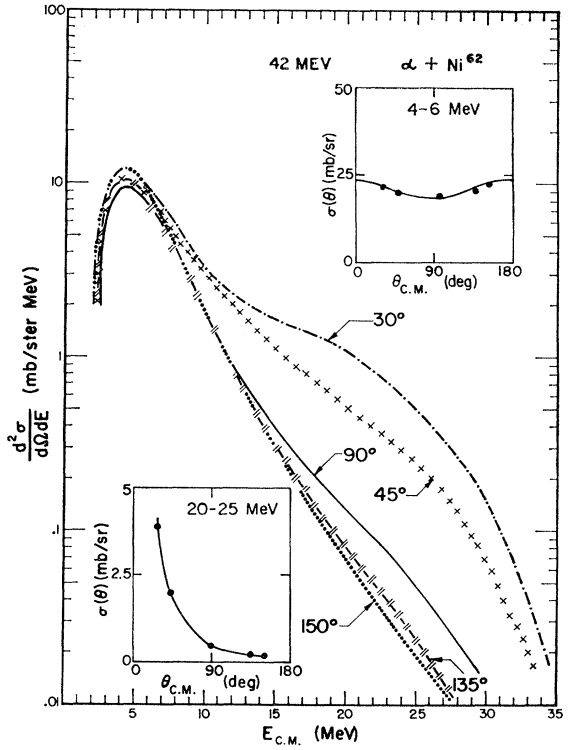

FIG. 9. Composite energy spectra for Ni^{62}. The insets show the angular distributions of a low-energy group and a high-energy group of protons.

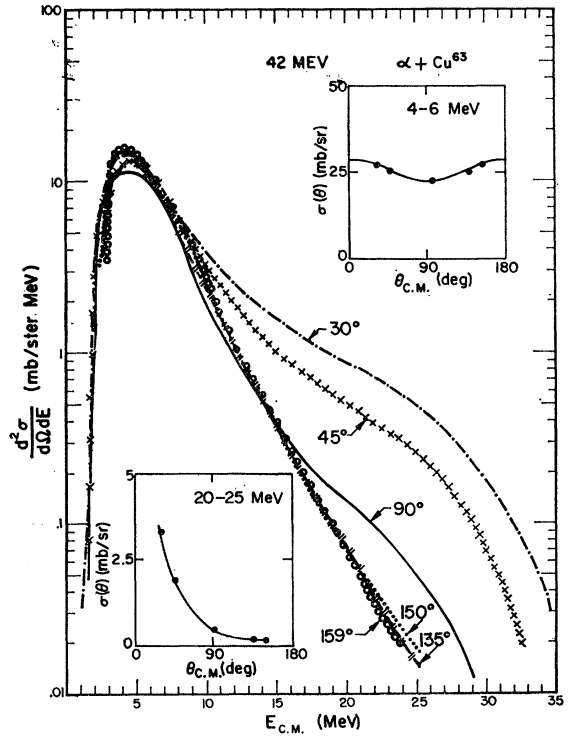

FIG. 10. Composite energy spectra for Cu^{63}. The insets show the angular distributions of a low-energy group and a high-energy group of protons.

spectra are slight, and in general, they do not greatly influence the results of general comparisons of spectra made between different energy and angular regions.

Composite energy spectra for each target have been produced by superimposing the smooth curves drawn from the data at each angle. An examination of these composite spectra (Figs. 6–15) and the accompanying insets suggest a natural grouping of the data into three regions based on target mass number: a region near $A=60$ (Co^{59}, Ni^{58}, Ni^{60}, Ni^{62}, Cu^{63}, Cu^{65}) which we will here call the nickel region, a region near $A=100$ (Nb, Rh, Pd) which we will call the rhodium region, and a region (actually a single point) near $A=200$ (Pt). (This division reflects the groupings in mass number of the

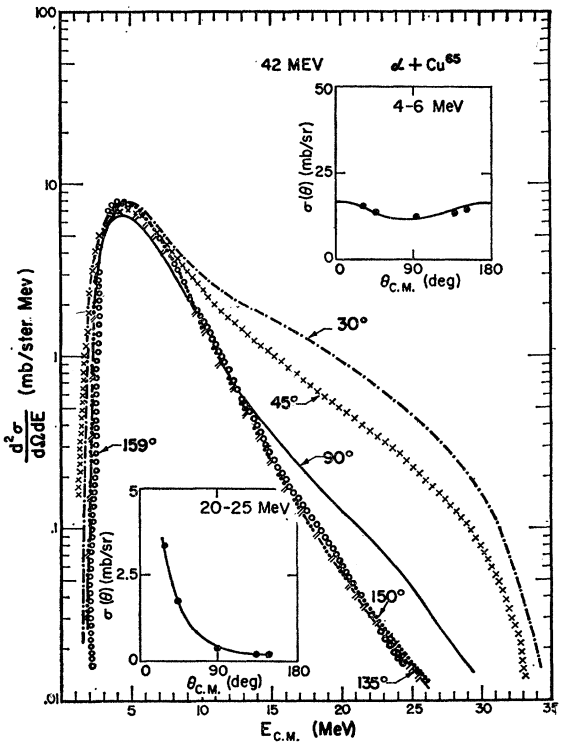

FIG. 11. Composite energy spectra for Cu^{65}. The insets show the angular distributions of a low-energy group and a high-energy group of protons.

targets used. Presumably the changes with A are gradual and, with more targets, the "regions" would blend into each other.) The total proton yield averages about 1000 mb in the Ni region, about 400 mb in the Rh region, and only about 50 mb for Pt. A second distinction between the regions is seen in the angular distributions of low-energy protons. In the Ni region they are symmetric about 90° with a minimum at 90°, in the Rh region they are rather isotropic with a possible small forward peaking, while for Pt they are all strongly forward peaked. The high-energy protons are strongly forward-peaked for all targets. The transition from sym-

metry at low energies to forward peaking at high energies is gradual, as illustrated in Fig. 16.

Another way of displaying the differences which exist is illustrated in Fig. 17 where we have plotted the energy spectra at angles of 30°, 90° and 150°. This figure shows that while the low-energy peaks at 30° vary in yield from target to target by a factor of 10, at higher energies near 20 MeV for example, the variance is only a factor of 2. If one ignores the somewhat anomalous behavior of Ni^{58}, the variation is only 30%. This relative constancy of the high-energy yield is not as pronounced at the backward angles as at 30°. Thus, although the high-energy part of the proton spectra is similar for all targets, the similarity is greatest where the absolute yield is greatest—at forward angles.

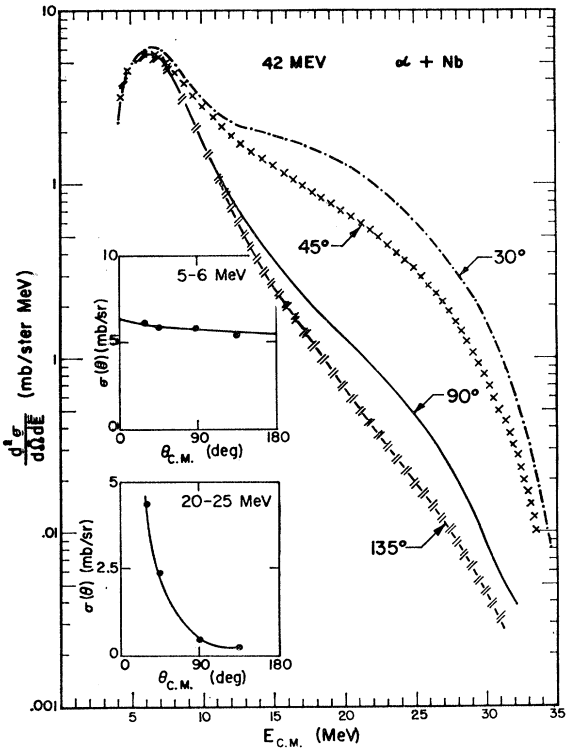

FIG. 12. Composite energy spectra for Nb. The insets show the angular distributions of a low-energy group and a high-energy group of protons.

The angular distribution of the total proton yield for each target is shown in Fig. 18. Such cross sections are the result of an integration of the entire experimental energy spectrum at each angle of observation. A further integration of the angular distributions results in the total cross sections for proton emission as measured in this experiment. These are listed in column two of Table III. All cross sections are absolute and while errors have not been shown for the cross sections at each angle in Fig. 18, Table III gives the over-all experimental uncertainty.

Essentially all the protons in the Rh and Pt regions

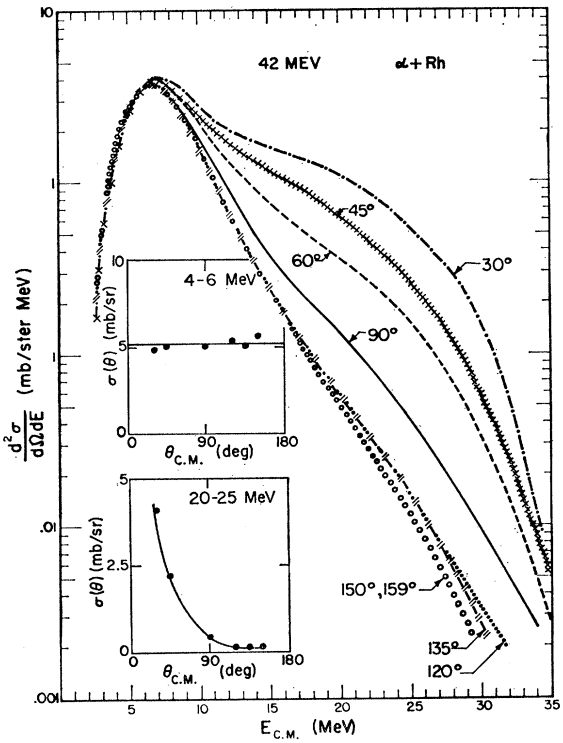

FIG. 13. Composite energy spectra for Rh. The insets show the angular distributions of a low-energy group and a high-energy group of protons.

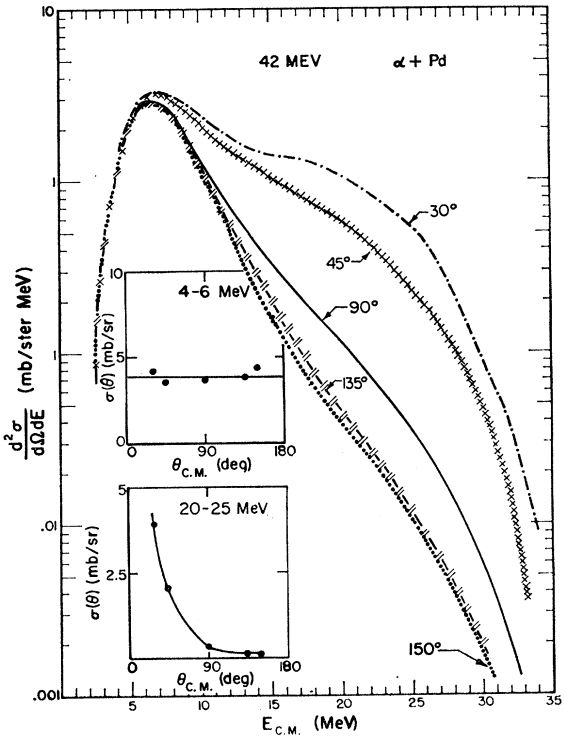

FIG. 14. Composite energy spectra for Pd. The insets show the angular distributions of a low-energy group and a high-energy group of protons.

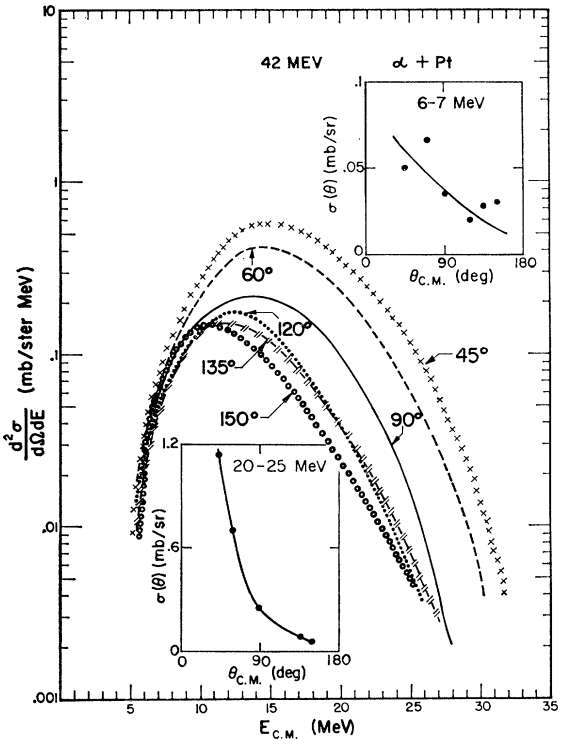

FIG. 15. Composite energy spectra for Pt. The insets show the angular distributions of a low-energy group and a high-energy group of protons.

and at forward angles in the Ni region were emitted with energies above the threshold energy of the proton detector. However, for the backward angle data in the Ni region, a non-negligible number of protons were below the threshold because of the motion of the center of mass. To account for these protons in the total cross section, the backward-angle data below 3.5 MeV was extrapolated to low energies on the basis of the energy spectra at forward angles. This procedure assumed that the 90° symmetry observed for protons just above the threshold could be extended to the unobserved protons.

IV. COMPOUND-NUCLEAR CASCADE CALCULATIONS

To correlate and interpret the data, it is useful to compare it with predictions of existing models of nuclear reaction processes. The statistical model of compound nuclear reactions has been applied with considerable success to reactions in this energy region,[1] and in its present form, makes quite detailed predictions concerning spectra, yields, and angular distributions. However, it is also well known that not all of the emission yield can be attributed to compound nuclear processes. The remainder is often designated by the term "direct interaction" process, although it has been suggested that besides these immediate events, taking place on a time scale comparable to nuclear transit times, there are also somewhat slower ones, sometimes called "intermediate."

At present, direct-interaction theory is not able to make detailed predictions concerning the distributions of emitted protons in reactions which leave the residual nucleus in a state of high excitation. In view of this difficulty and the strong suggestions of the data as presented in the previous section, we have chosen first to analyze the data by a comparison with the statistical theory of compound nuclear reactions.

In the Ni and Rh regions, the 90° symmetry of the low-energy group and the decrease of its yield with increasing Z, suggests that this part of the total proton yield is a result of a compound-nuclear evaporation. Although the high-energy protons are forward peaked, they show a tendency toward isotropy at angles greater than 120°. It might be tempting to assume that all of the 150° data (at least in the Ni and Rh regions) is "statistical." If this is done, values of the level-density parameter a can be found from the slope of a standard plot of

$$\frac{d^2\sigma}{d\Omega dE}\frac{U^2}{E\sigma_a} \text{ versus } \sqrt{U}.$$

The values of a found in this manner for Ni^{60}, Rh, and Pt are 6.5, 6.2, and 6.1, respectively, while the corresponding values for the common choice, $a=A/8$, are 8.0, 13.4, and 24.9. It should be noted that this apparent

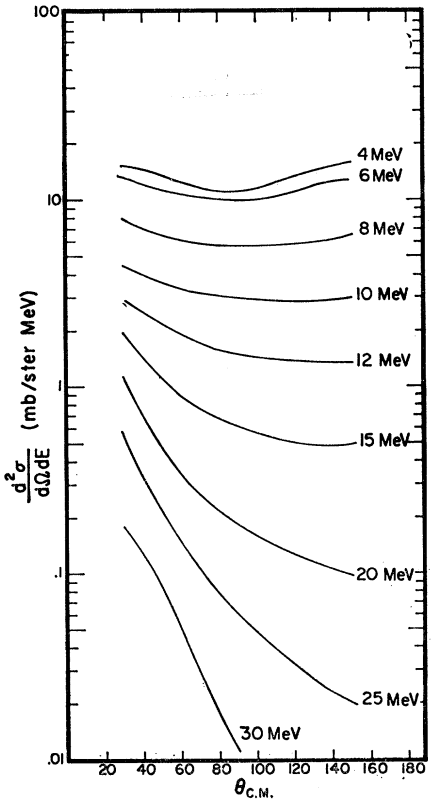

FIG. 16. Proton angular distributions at various energies for Co^{59}. All cross sections are absolute. The curves were drawn through data plotted for integral energies.

independence of the level-density parameter on the mass of the target has been observed by other investigators.[15–17] In the present data, this result could have been anticipated from the fact that the high-energy portions of the 150° spectra of Fig. 17 are approximately parallel for all targets. This indicates a common temperature and therefore a constant value of the level density parameter.

Although this behavior is in disagreement with current statistical theory, the proton spectra may still be the result of an "evaporation." Indeed, the behavior could be explained in terms of a nonequilibrium evaporation or "local heating" whereby a particle is emitted before complete thermal equilibrium is established. In such a process, only a fraction of the nuclear constituents would take part and the excitation of all available degrees of freedom would not be completely fulfilled. Discussions of this process, relating to the analysis of recent data, can be found in the literature.[17,28]

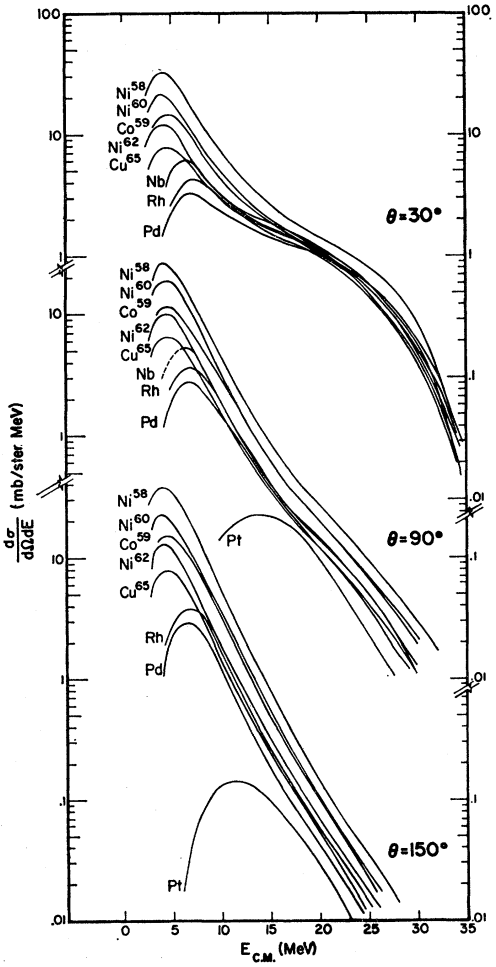

FIG. 17. Comparison of proton energy spectra at 30°, 90°, and 150°. All cross sections are absolute. Pt data were not collected at 30° and are not included at this angle. (The Cu^{63} data are omitted because its absolute cross section is in doubt.)

[28] V. A. Sidorov, Nucl. Phys. 35, 253 (1962).

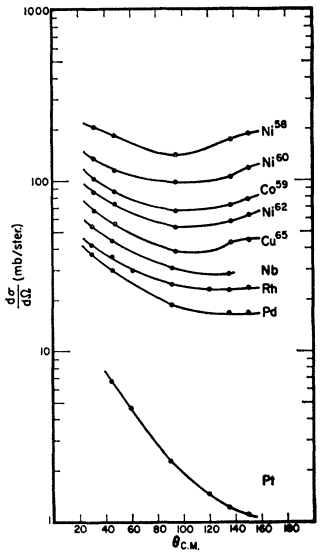

FIG. 18. Angular distribution of total proton yields.

However, there is another feature of the proton spectra at 150° which more seriously contradicts an evaporation mechanism. This is the fact that in the region where only first emissions can contribute, the magnitude of the slope of these spectra is constant or decreases from low to high energies. In contrast to this, a level-density expression of the form $(\exp\sqrt{U})/U^2$ requires the statistical-evaporation spectrum to have an ever steeper slope. In fact, this slope dependence is required for any model in which the temperature $T(U)$ is an increasing function of U. This disagreement between experiment and theory implies that the 150° proton yields cannot be considered as purely compound nuclear. It therefore argues against the possibility of arbitrarily "subtracting off" the 150° yield in an assignment of the data into a symmetric compound-nuclear component and a forward-peaked, noncompound-nuclear component.

For the present experiment, it was considered desirable to analyze the data without assuming that the backward yields were entirely compound-nuclear in origin. To this end, a statistical theory calculation was made to generate theoretical proton spectra. A comparison between these spectra and the data then formed the basis of estimating the fraction of the proton yield which is "statistical." The validity of this approach is examined below by a comparison of the observed spectra, yields and angular distributions with the implications of the calculation.

In this calculation described below, we have adopted a very simple model which neglects gamma-ray competition and any dependence of yields and spectra on the angular momentum of the emitting states or outgoing particles. The Monte Carlo calculations of Dostrovsky, Fraenkel, and Friedlander[2] (D.F.F.) indicate that the evaporation of particles other than alpha particles, neutrons, and protons is negligible, to a very good

approximation. Furthermore, these calculations[29] have shown that a majority of the alpha particles are emitted in the first stages of the cascade. Thus in this calculation we consider only nucleon emission and, where needed, correct for alpha emission by suitably scaling down the reaction cross section for the incident 42-MeV alpha particles. With these simplifications, the calculation reduces to finding the energy spectra and relative emission probability of neutrons and protons at each stage of the cascade.

The number of particles in an energy range dE of the spectrum of particles emitted from a compound nucleus, is according to the statistical theory (see, e.g., Weisskopf[30]).

$$N(E)dE=C_1E\sigma_c(E)\omega(U)dE, \quad (1)$$

where C_1 is a constant, E is the kinetic energy of the emitted particle, $\omega(U)$ is the level density as a function of the excitation energy U in the residual nucleus, and σ_c is the cross section for the inverse reaction.

On the basis of a Fermi-gas model, the level density can be shown to be of the form

$$\omega(U)=C_2U^{-2}e^{2(aU)^{1/2}}, \quad (2)$$

where C_2 is a constant, and a is the level-density parameter. This form of the level density, indicated by theory, has shown considerable agreement with experiment.[1] Pairing-energy corrections were made by replacing U with $U-\delta$ where δ is the sum of the pairing energies, P_Z and P_N.

Following the methods of Bodansky, Cole, Cross, Gruhn, and Halpern,[9] the relative emission probability of protons and neutrons can be shown to be given by

$$\Gamma_p/\Gamma_n=\exp[(B(Z-Z_0)+0.6-V')/T], \quad (3)$$

where Z_0 represents the charge at the center of the stable valley, B is a measure of the width of the stable valley, V' is the effective barrier to protons. T, the nuclear temperature, is given by the logarithmic derivative of the level density which gaves

$$1/T=(a/U)^{1/2}-2/U.$$

A number of quantities have been introduced into Eqs. (1)-(3) which must be evaluated before the calculation can proceed. Specifically we need to know the inverse cross section σ_c, the level-density parameter a, the pairing energies P_Z and P_N, and the values of B, Z_0, and V'. The source of each of these quantities is described below in the order in which they have appeared.

Neutron-reaction cross sections are rather independent of energy for neutron energies greater than 1 MeV, and therefore the neutron inverse cross sections were assumed to be constant throughout the cascade. Thus they play no part in determining the neutron spectral shape. This is a reasonable approximation here, as our only present interest in the neutron spectra is in the determination of the excitation energies for subsequent stages of the evaporation cascade. For protons, the reaction cross sections calculated by Shapiro[31] for a totally absorbing square-well potential were used in the determining of the spectral shape.

TABLE II. Cascade calculation parameters.

	Co^{59}	Ni^{58}	Ni^{60}	Ni^{62}	Cu^{63}	Cu^{65}	Nb	Rh	Pd	Pt
a	8.7	8.6	8.9	9.1	9.3	9.6	11.2	12.4	11.9	17.9
A_0	7	7	7	7	7	7	8	8.5	9	11
k	0.65	0.66	0.66	0.66	0.67	0.67	0.73	0.78		0.80
B			3.0				1.8	1.7		1.5
C_3			0.495					0.469		0.445
C_4			7.10					3.75		2.25

Values of the level-density parameter were based on the analysis of Lang (Ref. 11, Figs. 5 and 6). These values are listed in Table II along with their corresponding values of A_0. For a given cascade, the parameter a was taken as A/A_0, and thus a changed slightly as the cascade progressed. Lang's values were selected from particle spectra and neutron resonance data which involved nuclear excitations lower than those of the present experiment and there is reason to believe that the shell effects exhibited by these data should be of less significance at our higher excitations. The most pronounced shell effect is seen at the doubly closed shell of Pb and thus the value of the level density parameter for Pt which was taken from Lang may be grossly in error. Since it was found that the calculated compound nuclear contribution to the observed yield for Pt was small for all reasonable values of a, we cannot use the experimental results to determine the true value.

Although finding best-fit values of a was not one of the objectives of this experiment, it was found that by making a slight modification in the value selected for Pd, the same degree of agreement between the calculated and observed energy spectra was attained for all targets. For this reason, Table II lists a value of a for Pd which is lower than would have otherwise been prescribed. As a result of this slight modification, it is felt that all of the values of a listed in Table II (except for Pt where an *a priori* experimental assignment of the compound nuclear yield was not possible) are indistinguishable from what would have been selected as best-fit values, within an uncertainty of $\approx 10\%$. (Variations of a by more than 10% produced observable changes in shape which were not considered to improve the fit.)

Pairing energies were taken from values calculated by Cameron[32] and no attempts were made to modify them for shell corrections.

Values of B and Z_0, were taken from tabulations by Bodansky,[33] based on nuclear mass tables, where the variation of Z_0 with A could be represented by a func-

[29] Z. Fraenkel (private communication to D. Bodansky).
[30] V. F. Weisskopf, Phys. Rev. **52**, 295 (1937).
[31] M. M. Shapiro, Phys. Rev. **90**, 171 (1953).
[32] A. G. W. Cameron, Can. J. Phys. **36**, 1040 (1958).
[33] D. Bodansky (private communication).

tion of the form

$$Z_0=(C_3-C_4A\times10^{-4})A\,.$$

The constants C_3 and C_4 and the values of B used in the calculation are listed in Table II. The calculation used values of V' corresponding to a classical Coulomb barrier which were suitably reduced by a factor k to allow for barrier penetration:

$$V'=kV_c=kZe^2/r_0A^{1/3}$$

with a radius parameter $r_0=1.5\times10^{-13}$ cm. The factor k is taken from the work of D.F.F.[2] who used a barrier based on a fit of the classical expression for the reaction cross section to the continuum theory of Shapiro[31] (see Ref. 2, Table II). D.F.F. found these values of V' led to rather good fits of excitation cross sections over a wide range of A, and it also has been shown that they give good results for analyses of proton-yield measurements in the neighborhood of $A=60$. Thus their use here is based more on their empirical success in yield calculations, rather than on their correspondence to the shape of the Shapiro cross section.

Where needed, separation energies were taken from the 1960 Nuclear Data Tables[34] supplemented by values from Ashby and Catron,[35] and Seeger.[36]

There are many possible paths available in the flow of a cascade. Figure 19 shows the flow paths included in the calculation. With but one exception (the flow *n-n-n-p*), the paths involved the emission of three particles. Sample calculations showed that four-particle emission was highly improbable at excitation energies reached in 42-MeV alpha-particle bombardments.

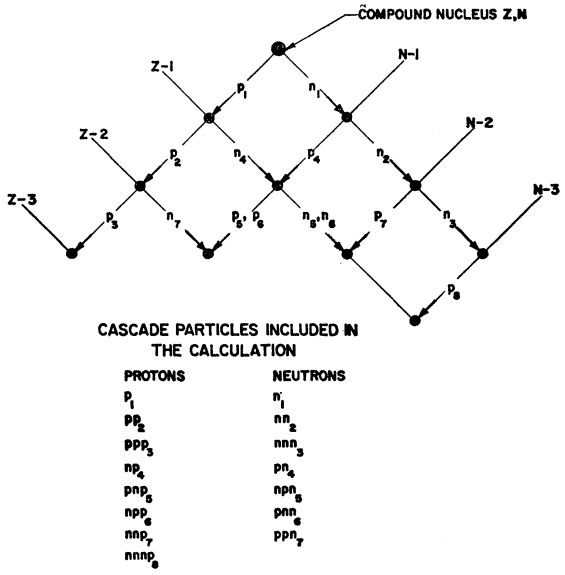

FIG. 19. Flow diagram of protons and neutrons included in the compound-nuclear cascade calculation.

The calculation proceeded as follows: Proton p_1 was emitted by the initial compound nucleus (Z,N) with its energy spectrum and the resulting residual excitation energy spectrum of $(Z-1, N)$ given by Eq. (1). These spectra, sectioned into 1-MeV energy bins, were separately summed and renormalized to a total area of Γ_p. The lower limit of the sum was determined by the restriction $U\geq4/a$. This limit for the residual excitation energy corresponds to the minimum in the expression for the level density (which approaches $+\infty$ as $U\rightarrow0$ although the level density itself decreases monotonically as $U\rightarrow0$). Since this minimum occurs at $U<0.5$ MeV for $a\geq8$, this low-energy cutoff does not represent a serious restriction.

In the next step, each bin of excitation energy in the nucleus $(Z-1, N)$ became the source of a second generation of protons (and neutrons) and the above procedure was repeated. The spectrum resulting from a given generation (other than the first) was therefore the result of the sum of spectra for each energy bin of excitation in the generating nucleus. When only one particle was above the emission threshold, its relative width was set equal to 1 (ignoring gamma-ray competition).

The calculation continued through the pre-arranged sequence of nuclei listed in Fig. 19 until all contributing protons and neutrons had been added to their respective spectra. The resulting 8 proton, 7 neutron, and 10 nuclear-excitation energy spectra were stored in a computer (an IBM 709) and were available to the output in the form of protons per MeV per cascade. The total proton and total neutron spectra were also computed along with the values of the sums of these 17 emission spectra. The entire procedure took ≈20 sec of computer time. Because Pd and Pt were multi-isotopic targets, the calculation produced composite spectra of their major isotopes weighted by their natural abundances. Five isotopes of Pd and four isotopes of Pt were included in their respective composite spectra.

V. COMPARISON OF CALCULATED AND OBSERVED DISTRIBUTIONS AND YIELDS

Figure 20 presents a comparison of the shape of the predicted compound-nuclear proton spectrum and the observed proton spectrum for Co^{59}. Cobalt-59 is chosen as an illustrative case because it somewhat typifies the situation in the Ni and Rh regions.

In the present comparison of spectral shapes we have chosen not to normalize the calculation on an absolute scale but rather to normalize it directly to the observed spectrum. As will be seen below, this latter method of normalization is adopted for all the targets except Pt and then compound-nuclear yields obtained by both methods of normalization are compared.

[34] I. A. Koenig, J. H. E. Mattauch, A. H. Wapstra, and F. Everling, *1960 Nuclear Data Tables* (U. S. Government Printing Office, Washington, D. C.), Parts 1 and 2.

[35] V. J. Ashby and H. C. Catron, University of California Radiation Laboratories Report No. UCRL-5419, 1959 (unpublished).

[36] P. A. Seeger, Nucl. Phys. **25**, 1 (1961).

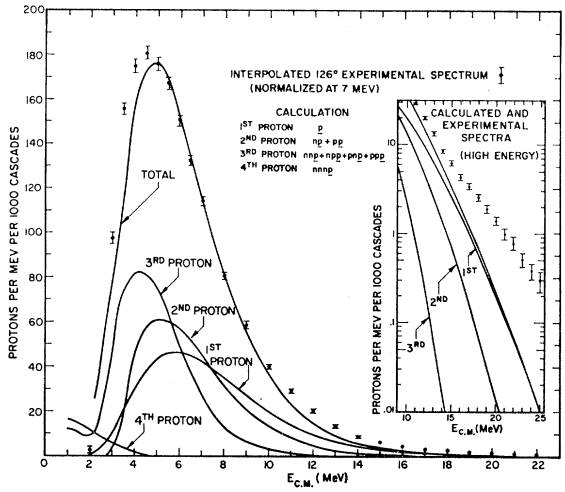

FIG. 20. A comparison of the calculated and experimental proton energy spectra for Co^{59}. The experimental data (dots) have been interpolated for a center-of-mass angle of 126° in an attempt to simulate an average angle (see text). The experimental excess at high-energy protons (inset) is attributed to a nonstatistical process while the low-energy excess is attributed to inadequacies in details of the statistical model calculation.

The fact that appreciable anisotropies exist in the low-energy portion of the Ni-region data complicated the comparison of the calculated and observed spectra. This is because the calculation, ignoring all angular-momentum effects, produces spectra based on complete isotropy of the compound-nuclear yield. Both classical[37] and quantum mechanical[38] calculations, have shown that the anisotropy should be described by an angular distribution proportional to $(1+X\cos^2\theta)$. As a first-order attempt to eliminate angular-momentum effects in the low-energy data, we have interpolated on the basis of this distribution the experimental data for Co^{59} at an angle where $\cos^2\theta$ is equal to its value averaged over the sphere. The distribution at this angle [at which $P_2(\cos\theta)=0$; or $\theta\approx 126°$] should correspond to an "effective average" distribution. This procedure tacitly assumes that angular-momentum effects do not change the energy of the evaporated protons but simply redistribute their angular distribution realtive to the beam direction.

The calculated and interpolated spectra, which were normalized to coincide at 7 MeV, match in shape for the energy range ≈ 5.0 to ≈ 9.5 MeV, with the observed spectra exceeding the calculated spectra for both lower and higher energy protons. Generally speaking, the calculated and experimental spectra coincided over the largest energy ranges for those targets and at those angles for which the relative compound-nuclear yield was the largest. That is, the degree of correlation between the calculated spectrum and the experimental spectrum improved when the expected relative number of non-compound-nuclear events decreased. In all comparisons of the calculated and observed spectra, protons above an energy of 12 MeV were more abundant in the observed spectra than in the calculated spectra at all angles of observation. If we assume that the low-energy protons are from an evaporation mechanism, and that we have correctly compensated for the anisotropy, then the differences in the observed and calculated spectra at low energies must be attributed to inadequacies of the calculation.

It was first thought that an improved agreement could be effected by using a barrier more transparent to low-energy protons—for example an optical-model barrier. Since these original calculations were made, proton-reaction cross sections based on an optical-model potential have been calculated by Mani, Melkanoff, and Iori.[39] A comparison of these cross sections with the cross sections calculated by Shapiro for a totally absorbing square well showed them to be quite similar in energy dependence especially at low proton energies. A sample calculation of the cascade for the Ni-region elements using inverse cross sections fitted to the Mani, Melkanoff, and Iori optical-model data showed that only slight changes in the spectral shape at low energies would result from their use. For these reasons, a more thorough calculation was not attempted.

Another possible cause of the disagreement, namely our neglect of other than nucleon emission, was investigated when a computer code which could include or exclude alpha-particle emission was used for a test calculation of the cascade for Ni^{58}. The code, which was made available by Marshall Blann and is described elsewhere,[14] showed that the inclusion of alpha-particle emission reduced the proton-energy spectra by about the same factor (35%) at all energies and as such made only very minor changes in the shape of the proton-emission spectrum.

Thus neither the use of inverse cross sections based on an optical-model potential nor the inclusion of alpha-particle emission seems to increase noticeably the relative number of low-energy protons in the calculated spectrum. While the true reason or reasons for the lack of agreement between the cascade calculation and the experimental yield at low energies is not known, it is believed that angular-momentum effects which give rise to the pronounced anisotropies in the Ni region may play an important role. The possible role of angular-momentum considerations is consistent with the generally better correspondence between calculation and experiment in the Rh region where the low-energy protons indicate an isotropic rather than anisotropic angular distribution. This feature is shown in Fig. 21 where we compare the calculated and experimental spectra for Ni^{58}, Rh, and Pt. (The calculation has been normalized to the experimental yield at 7 MeV for Ni^{58} and Rh. However, the Pt normalization is a result of the use of

[37] T. Ericson, and V. Strutinski, Nucl. Phys. **8**, 284 (1958).
[38] A. Douglas and N. MacDonald, Nucl. Phys. **13**, 382 (1959).
[39] G. S. Mani, M. A. Melkanoff, and I. Iori, Commissariat à L' Énergie Atomique, Report No. CEA-2379, 1963 (unpublished).

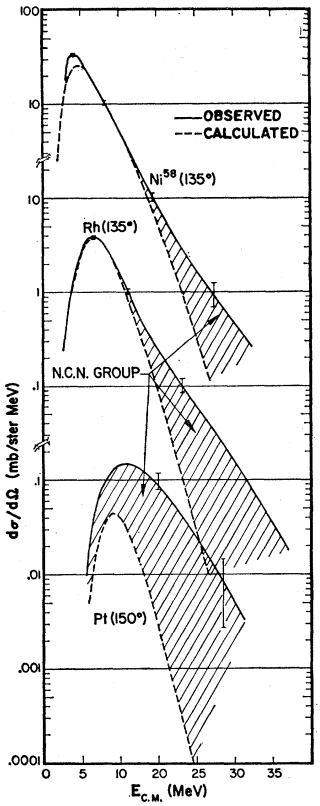

FIG. 21. A comparison of the calculated and observed proton spectra for Ni^{58}, Rh, and Pt. The observed cross sections are absolute. For Ni^{58} and Rh, the calculation was normalized to the observed spectra at 7 MeV. The calculated spectrum for Pt was normalized to a "corrected" reaction cross section for incident 42-MeV alpha particles (see text). Noncompound-nuclear events are indicated by the shaded areas.

the reaction cross section for the formation of the compound nucleus as described below.)

The calculated spectra are thus seen to provide a qualitative explanation at the observed spectra below about 9 MeV with a good match in shape from about 5 to 9 MeV. We then assume that noncompound-nuclear events are confined only to higher energies. Thus a subtraction of the calculated spectrum from the experimental spectrum in the region above 9 MeV separates the proton yield into a compound-nuclear and a noncompound-nuclear portion. The noncompound-nuclear portion is indicated by the shaded areas in Fig. 21 for Ni^{58}, Rh, and Pt. This procedure further assumes that at and below the region where the calculated and experimental spectra coincide (in the Ni and Rh regions), the entire experimental yield is due to compound-nuclear events. On the basis of just such an assumption, we have tabulated the "experimental" noncompound-nuclear (NCN) and compound nuclear (CN) yields in columns 3 and 4 of Table III. These yields are labeled as "experimental" to emphasize the fact that they are based on a normalization of the cascade calculation to the experimental spectra and also that at low energies, which account for most of the cross section, the entire experimental yield was assumed to be compound nuclear.

In the Ni region, the normalization was made at 135° since this most closely corresponded to the effective average angle of 126°. In the Rh region where no anisotropy was observed in the experimental data, the calculated spectrum was normalized to the most backward angle of observation. For Pt, an experimental normalization of the calculation could not be made with confidence at any angle, and thus for Pt, no "experimental" yields have been listed.

TABLE III. Proton cross sections (mb).

	Total cross section	"Experimental" NCN	"Experimental" CN	"Calculated" CN	CN "Expt" / CN "Cal"
Co^{59}	970±70	89	881±40	870±40	1.02
Ni^{58}	2070±200	116	1954±190	1740±70	1.12
Ni^{60}	1330±200	94	1236±185	1220±50	1.01
Ni^{62}	774±80	89	685±70	720±30	0.95
Cu^{63}	975±60[a]	75[a]	900±55[a]	1360±50	0.66[a]
Cu^{65}	580±60	75	505±52	630±30	0.80
Nb	440±40	85	355±35	410±20	0.87
Rh	360±30	94	265±22	250±10	1.05
Pd	284±20	77	207±14	190±10	1.07
Pt	47.5±10	...	...	2.9±0.1	...

[a] Possibly 30% too small because of target-thickness error.

If the assignment of compound-nuclear and noncompound-nuclear components is valid, one should be able to account for the absolute yields and angular distributions of the compound-nuclear component in terms of the statistical model. We first consider the yields. Theoretical values of the CN cross sections based on corrected total cross sections for 40-MeV alpha particles are listed in column 5 of Table III, under the heading of "calculated" CN. These values were found by multiplying the number of protons per cascade computed by the cascade calculation by the "corrected" alpha-particle cross sections. Corrections for direct interactions and alpha-particle emission were made to interpolated values of the experimental reaction cross sections for 40-MeV alpha particles measured by Igo and Wilkins.[12] [We have assumed that σ_{CE} is small and that the reaction cross section is equal to the tabulated values of $(\sigma_R - \sigma_{CE})$ in Ref. 12.] The errors are based on those assigned by Igo and Wilkins to their reaction cross sections. The assignment of direct-interaction corrections were based on the forward-peaked proton yields of the present experiment and the forward-peaked neutron yields observed by Drake[40] [42-MeV (α,n) on Co^{59}, Nb, and Au]. Typical direct cross sections were 160 mb for the Ni region, 210 mb for the Rh region, and 140 mb for Pt. Since other direct interactions for incident 42-MeV alpha particles were found difficult to estimate and are considered to be small, no further direct-interaction corrections were made.

As mentioned earlier, the calculation neglected other than nucleon emission and we here make corrections for alpha-particle evaporation (the next most probable emitted particle) by reducing the cross section for compound-nuclear formation. Whereas alpha-emission corrections based on the Monte Carlo calculations of D.F.F were avaliable for the Ni region,[29] it was necessary in the Rh region to base alpha-emission estimates on an extrapolation of the (α,n) excitation function data for

[40] D. Drake (private communication).

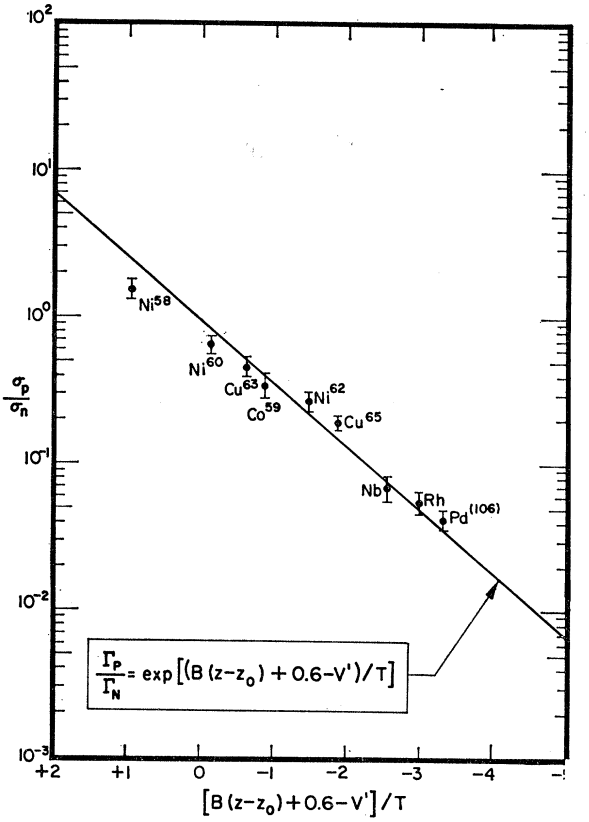

FIG. 22. Ratio of proton to neutron yield as a function of "proton richness." The abscissa is evaluated for "first-emission" protons. σ_p is the experimental compound nuclear proton cross section (column 4, Table III). σ_n for Co^{59}, Nb, Rh, Pd, and Pt is based on the measurements of Drake. All other values of σ_n come from D.F.F.

Rh.[41] These corrections were 300 to 400 mb in the Ni region, 50 to 70 mb in the Rh region, and zero for Pt.

The ratios of the "experimental" and "calculated" CN cross sections are listed in column 6, and with the exception of the Cu isotopes, they show agreement to within the assigned errors. Although the 34% disagreement for Cu^{63} cannot be explained with certainty, we believe it is probably due to an error in the target-thickness determination. The obvious alternative of accepting it as evidence of a true anomaly in the cross section appears unreasonable in view of the success of the other yield calculations, and the indications of errors in the Cu^{63} target thickness. The disagreement for Cu^{65} cannot be similarly explained since it is felt that the experimental error includes a correct assignment to the error in the target thickness. If we assume that the error assigned by Igo and Wilkins to the total cross section, used for the "calculated" yield is correct, then it must be concluded that either the cascade calculation overestimated the proton yield for Cu^{65} or the experimentally measured value is too small. The true cause is not known.

[41] S. Tanaka (private communication to D. Bodansky).

Except for Cu, the general agreement between the "experimental" cross sections based on a normalization of the cascade calculation to experimental alpha-particle reaction cross sections, supports the assignment of the compound-nuclear portion of the observed proton yields in the Ni and Rh regions. In extending the analysis, we have calculated the expected compound-nuclear proton yield for Pt to be 2.9 mb, and this value has been listed in column 5 of Table III. This "calculated" value for the compound-nuclear yield accounts for only 6% of the observed total proton yield and is therefore consistent with a predominantly direct interaction nature of the Pt cross section. It is also less than 4π times the observed yield at 150° (giving a total yield of 11 mb), which should be an upper limit of the compound nuclear yield for Pt.

The value of the level-density parameter used in the calculation of the Pt yield came from neutron-resonance data included in the review by Lang. At the higher excitation energies of the present experiment, it is expected that the level-density parameter should be less dependent upon the shell effects exhibited by these resonance data. For the calculated yield listed in Table III, we have used a value of a equal to 17.9. A somewhat different value ($a=22.5$) was reported by Drake[3] for the (α,n) spectra of Au resulting from bombardments by 42-MeV alpha particles. Since this experiment is more closely related to the present (α,p) experiment, it is instructive to compare the results when this larger value of a is used in the yield calculation for Pt. For $a=22.5$, the value calculated for the cascade is 2.2 mb as compared to the value of 2.9 mb listed in Table III for $a=17.9$. Although this is a 28% change in the CN yield for Pt, it is only a 2% change in the CN contribution to the total yield, and it therefore does not appreciably change the results.

The consistency of the experimental compound-nuclear yields with statistical theory expectations can be displayed in a second way, which does not rely on the details of the cascade calculation. Here we examine the correlation between the experimental proton-emission probability (expressed through the ratio σ_p/σ_n) and the position of the emitting compound nucleus with respect to the stable valley of isotopes. In Fig. 22, we have plotted (σ_p/σ_n) as a function of a parameter describing "proton richness" [see Eq. (3)]. σ_p is the total proton CN cross section as measured in this experiment (column 4, Table III). Values of σ_n for Co^{59}, Nb, and Au as measured by Drake[3] were used for Co^{59}, Nb, and Pt, respectively, and the Nb value was extrapolated to Rh and Pd. All other values of σ_n were taken from the predictions of D.F.F.[2]

For purposes of simplicity and consistency, the abscissa $[B(Z-Z_0)+0.6-V']/T$, was evaluated for a "first emission" from the initial compound nucleus for all targets. This assumes that the first emission typifies the average value of σ_p/σ_n for the cascade. In general, the cascade should flow in a direction that causes σ_p/σ_n

to approach unity or the abscissa to approach zero. This would cause the point for Ni^{58} to shift to the right while all other points would be shifted to the left in Fig. 22. Opposing these shifts is the decrease of temperature, T, associated with the "cooling" of the nucleus as the cascade progresses.

The values of σ_p/σ_n for Co^{59} and Nb are primarily experimental since σ_n is based on the experimental measurements of Drake, and σ_p is the result of normalizing the cascade calculation to the experimental proton spectra of this work. This is also true of the Rh and Pd points to the extent that these values of σ_n were extrapolated from the results of Drake. In calculating the abscissa for Pd, Pd^{106} was taken to represent the average of its naturally occurring isotopes.

As discussed above, B and Z_0 are not adjustable parameters, but are empirically determined from tabulated values of separation energies. Although T, the temperature, could be considered as somewhat adjustable, it is not a completely free parameter since it must conform to the results of numerous other experiments. In the present analysis, its value has been predetermined through its dependence on the level density parameter, the values of which have been selected (with a slight adjustment for Pd) from the analysis of Lang.[11] The one remaining parameter (V'), the effective barrier, could have been considered as free. As stated above, we chose to predetermine its value from the recipe of D.F.F.[2] The fact that the "experimental" yields, plotted in Fig. 22, i.e., Co^{59}, Nb, Rh, and Pd, show a close correlation with proton richness, confirms that the recipe for V' is a satisfactory one. This should not be too surprising considering the relative success of the analysis by D.F.F. The existence of a recipe for V', which according to Fig. 22 has been shown to work in the relatively wide mass region between $A=58$ and $A=106$, gives one some confidence in extending the calculation to higher mass regions where an experimental assignment of the small compound-nuclear proton yield is not possible.

A second test of the compound-nuclear assignment comes from the prediction of the statistical model that emission spectrum is symmetric about 90° in the center-of-mass system. The cascade calculation, in ignoring all angular momentum effects, is incapable of directly contributing information pertaining to the shape of the angular distributions of the CN yields. Because the CN spectrum has been assigned as the calculated spectrum at high energies (above ≈9 MeV), we are tacitly assuming that the angular distribution of the high-energy CN protons is isotropic. In the Ni and Rh regions, the CN spectrum has been assigned as the experimental spectrum below ≈7 MeV and thus the experimentally measured yield dictates the angular distribution's symmetry in this region. In the Rh region, these experimentally measured low-energy events constitute more than 65% of the entire angular distribution (CN+NCN) while in the Ni region, they contribute more than 80% of the

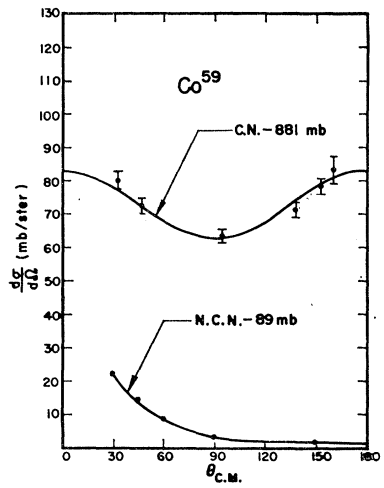

FIG. 23. Angular distribution of non-compound-nuclear (NCN) and compound-nuclear (CN) protons for Co^{59}. The identification of the NCN yield at each angle is based on the difference between the observed and calculated spectrum for high-energy compound-nuclear events (see Fig. 20). The CN yield includes all other events. The solid line drawn through the CN yield is a fit of the CN data to an expression of the form $(1+X\cos^2\theta)$.

entire angular distribution. It would therefore be anticipated that the angular distribution of the CN yields should be similar to those exhibited for events between 4 and 6 MeV as shown in the insets of Figs. 6 to 14. This was indeed found to be true for all the targets and representative samples have been reproduced here for Co^{59}, Rh, and Pt. These are plotted in Figs. 23–25, respectively, where the angular distribution of NCN events have been included for comparison.

The angular distributions of the CN yields in the Ni and Rh regions (here typified by Co^{59} and Rh) were all found to be symmetric about 90°. In the Ni region, there is forward and backward peaking for the CN component, while in the Rh region, this component is isotropic. For Pt, no experimental assignment was made of the CN part of the spectrum and therefore there is no experimental information bearing on the CN angular distribution. The line drawn for the Pt CN yield is due entirely to the cascade calculation.

While this symmetry about 90° for CN yields in the Ni and Rh regions is a confirmation of the validity of the division into CN and NCN components, it does not necessarily add any creditability to the calculation. In essence it reflects the fact that the experimental yield below 7 MeV is symmetric about 90° and hence this yield is very likely due to CN emission.

The curve drawn through the CN yield for Co^{59} in Fig. 23 is a result of a least-squares fit of the data to a distribution given by

$$\sigma=\sigma_{90}(1+X\cos^2\theta), \qquad (4)$$

which is the predicted form of the distribution based on both classical[37] and quantum-mechanical calculations,[38] of evaporation from a rotating system when the anisot-

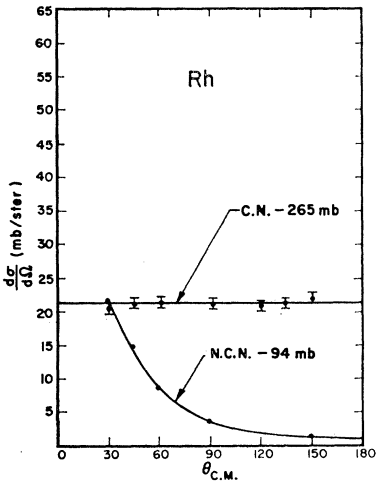

FIG. 24. Angular distribution of noncompound-nuclear (NCN) and compound-nuclear (CN) protons for Rh. The identification of the NCN yield at each angle is based on the difference between the observed and calculated spectrum for compound-nuclear events (see shaded area of Fig. 21). The CN yield includes all other events.

ropies are small. Values of X, the anisotropy coefficient for the total CN yields of targets in the Ni region are plotted as crosses at the top of Fig. 26. (The other points of Fig. 26 are discussed later.) The error bars represent a realistic estimate of the experimental uncertainty for the average anisotropy coefficient for each target. The weighted average of these five values is 0.34 ± 0.07.

Although the model upon which Eq. (4) is based predicts similar values of X for nuclei of nearly the same mass and radius, it would be an oversimplification to assume that X should be identical for all six targets. One reason for this is that the last proton probably makes the greatest contribution to the anisotropy (see, e.g., Lassen and Sidorov[10]) and the relative number of last protons from the different targets is not the same. However, the differences in the percentages of last protons are believed to be small and while a gradual change from target to target is possible, large changes in X from target to target are not expected. There is therefore some concern as to the interpretation of the relatively high value of X for Ni^{58}.

While this value of $X(0.43\pm0.08)$ agrees well with that found by Bodansky, Cole, Cross, Gruhn, and Halpern,[9] (0.39 ± 0.04), a meaningful comparison of the anisotropy coefficient between these two experiments is complicated by the fact that the latter was made at a lower incident energy (32 MeV) and involved only those events in which at least two protons were emitted.

In the Rh region, we find the total CN yield to be isotropic (see the example of Fig. 24). However, the relatively higher precentage of NCN protons in this region could mask the presence of a small anisotropy. The general trend of a decreasing value of X for increasing mass as observed by Drake[3] [42-MeV (α,n) on Al, Co^{59}, Nb, and Au] coincides with the results of the present experiment which shows anisotropies in the Ni region giving way to isotropy in the Rh region. This trend is qualitatively explained by the increased moment of inertia of the heavier nuclei which allows slower rotational velocities for the same amount of angular momentum.

A more detailed analysis of the anisotropy in the Ni region is presented in the lower portion of Fig. 26, where we have plotted the anisotropy coefficient for a number of energies near the peak of the experimentally measured composite spectra of Figs. 6–11. (In all calculations of the anisotropy, corrections were made for the difference between the laboratory and the center-of-mass angles.) The error bars shown are the standard deviations as given by the least-squares fit of the data to Eq. (4). The values of X are all less than 1.0 and have averages which range from a low of ≈0.2 for Ni^{60} to a high of ≈0.4 for Ni^{58}. Except for Cu^{65}, the points show a tendency toward increasing anisotropy with decreasing emission energy. This effect was also observed by Drake[3] for neutrons from Al, Co^{59}, and Nb, and was qualitatively explained in terms of two additional effects: (a) The alpha particle's kinetic energy in the center of mass must be shared between excitation energy and rotational energy. As a result, nuclei with the greatest rotational energy (large X) also have the least excitation energy and hence contribute most strongly to the low-energy portion of the spectrum. (b) A decreasing nuclear moment of inertia with decreasing excitation energy[42] increases the effective rotational energy in the later stages of the cascade, causing an increase in X for

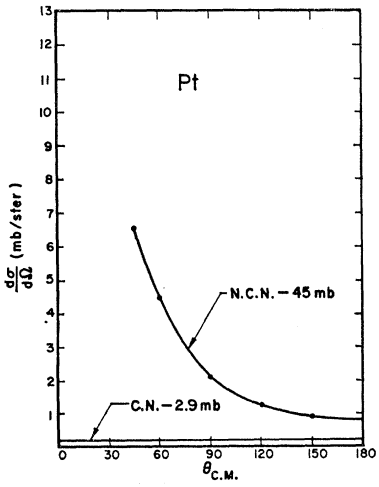

FIG. 25. Angular distribution of non-compound-nuclear (NCN) and compound nuclear (CN) protons for Pt. The CN yield was assumed isotropic and its yield was assigned by the cascade calculation normalized to the reaction cross section for 42-MeV alpha particles. A subtraction of this CN yield from the observed yield at each angle gave the cross section for NCN events.

[42] See, for example, the experimental evidence cited in Ref. 1.

those stages which contribute most to the low-energy emissions.

VI. NON-COMPOUND-NUCLEAR EVENTS

We turn now to a closer examination of the non-compound-nuclear events as previously defined by the difference between the calculated and observed spectra and indicated by the shaded area of Fig. 21. The total NCN yield for each target has been listed in column 3 of Table III. These yields are the result of an integration of angular distributions exemplified by Figs. 23–25. The shape of the NCN angular distributions is not known for angles less than 30° since complete energy spectra were not obtained in this region. As the solid angle corresponding to $\theta<30°$ is small, the total-cross-section estimate should be relatively insensitive to errors in a smooth extrapolation of the distribution.

Sample energy spectra for the NCN component have been plotted in Figs. 27–29 for Co^{59}, Rh, and Pt. Again Co^{59} and Rh represent the general results in the Ni and Rh regions, respectively. Because the CN yield for Pt lacks the experimental verification available to the other targets, its assignment is less relaible. Furthermore, this calculated value is less than 6% of the total Pt yield. It might therefore be reasonable to consider the Pt data as totally direct and examine it as such. We have chosen instead to subtract the calculated CN spectrum from the data. The reasons for this choice are as follows: (1) This is consistent with the procedure followed for all other targets; (2) The CN component is already small, the results would not be appreciably different if it has been overestimated; (3) If the CN yield has been underestimated, this subtraction is at least in the right direction; (4) On the basis of the substantial agreement of the calculation for the other targets, it seems reasonable to hope that the calculation gives a realistic value for Pt.

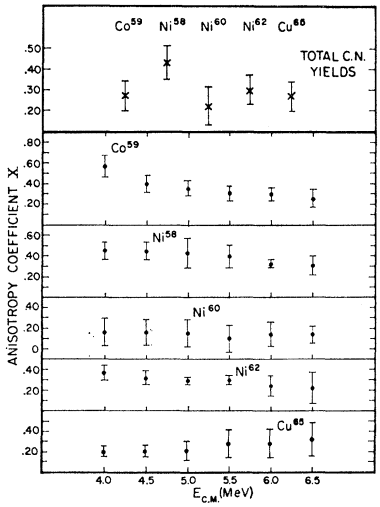

FIG. 26. Anisotropy coefficients. The anisotropy coefficients were found from a least-squares analysis of the angular distribution of the total CN yield (crosses) and of the CN yield at various energies (dots). The analysis was based on an angular distribution of the form $(1+X\cos^2\theta)$. The error bars for the total yields are probable errors based on experimental uncertainties. All other error bars represent standard deviations of the anisotropy coefficients as found from the least-squares analysis.

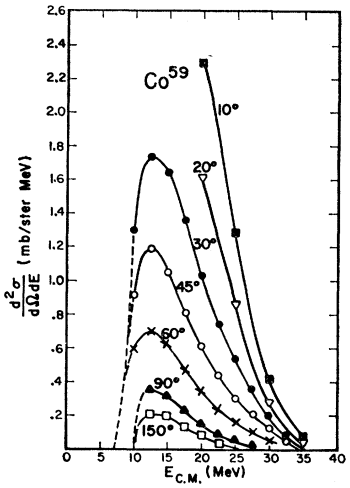

FIG. 27. Energy spectra of NCN protons for Co^{59}. The identification is based on the difference between the observed spectrum and the calculated spectra for compound-nuclear events. The dashed portion reflects the uncertainty in the low-energy threshold.

An examination of the NCN events reveals the following:

(a) The energy spectra of the NCN protons are strikingly similar in shape for all the elements studied. It is noted that comparisons of these spectra in their low-energy regions should be made with caution because at low energies the NCN component comprises a very small fraction of the total yield and is therefore sensitive to errors in both the experimental data and the CN calculation. For this reason, we have used a broken line in the low-energy regions of Figs. 26 and 28. (It is estimated that these errors contribute a relative uncertainty of less than 10% to the total NCN yield listed in Table III.) On the other hand, for the high-energy data ($E>20$ MeV), and especially at forward angles, the NCN protons dominate the yield. In this energy region, the data at 30° as plotted in Fig. 17 illustrated the similarity in the shape of the NCN spectra for each target. Considering the Pt data at 30° to be the "purest" example of a NCN energy spectrum, its shape, as plotted in Fig. 15, broadly peaks at an energy above the classical proton Coulomb barrier (13 MeV for $r_0=1.5$). The shift of the peak position to lower energies at backward angles could quite possibly be caused by the presence of an isotropic CN component which peaks at a lower energy (the calculated CN spectrum peaks at $\approx$9 MeV) and which is relatively small except at backward angles. However, we interpret this shift as a property of the NCN spectrum, and note that it still persists in Fig. 29, where the CN component has been subtracted. This shift of the peak position to higher energies at forward angles is consistent with the fact that the higher energy NCN protons are more strongly peaked in the forward direction.

(b) The total NCN yield remains relatively insensitive to the mass of the target. Although slightly higher for Ni^{58} and lower for Pt, the total NCN yield is approximately constant at 80 to 90 mb for all elements studies. The difference of a little more than a factor of 2 between Pt and Ni^{58} NCN cross sections is small in comparison to the 3 orders of magnitude difference in their respective CN yields. In particular, neither the target Z nor the reaction Q values have much effect on the NCN yields.

(c) The NCN protons are strongly peaked in the forward hemisphere. In Ni^{60}, for example, the yield at 30° is 25 mb/sr while that at 150° is only 1.8 mb/sr.

(d) Although the relative contribution of NCN protons may be small at some angles, it is never insignificant. For example, the 1.8 mb/sr NCN cross section for Ni^{60} at 150° contributes less than 2% to the total proton yield at this angle, and yet it still dominates the energy spectrum above 15 MeV. This effect is even more pronounced in the Rh region and especially in the Pt region where the CN cross sections are considerably smaller.

It should be emphasized that while we rely on the cascade calculation to make a quantitative estimate of the NCN component (by subtraction), the over-all features described above, (a)–(d), will not be altered much by small changes in the shape of the calculated spectrum.

VII. CONCLUSIONS AND SUMMARY

In the forgoing treatment of the experimental results, we have tended to consider the data as being composed of two distinct groups, a reasonably well-understood compound-nuclear group and a "leftover" noncompound-nuclear group. We have attempted to justify the validity of this approach by examining the degree to which the extracted compound-nuclear group conforms to the predictions of the statistical model in relation to energy spectral shapes, angular distributions, and yields. Good agreement was found for all three aspects: the calculated and experimental spectra match in slope over a reasonably wide energy range; the angular distributions are symmetric about 90°, and are consistent with evaporation from a rotating system; the yields agree well with predictions of a cascade calculation and relative yields for different targets make sense according to the proton richness recipe. The over-all agreement lends support to the identification of the "leftover" group as arising from mechanisms other than statistical emission from an excited compound nucleus.

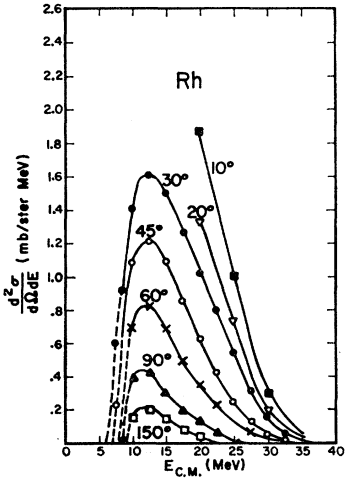

FIG. 28. Energy spectra of NCN protons for Rh. The identification is based on the difference between the observed and the calculated spectra for compound-nuclear events (see Fig. 21). The dashed portion reflects the uncertainty in the low-energy threshold.

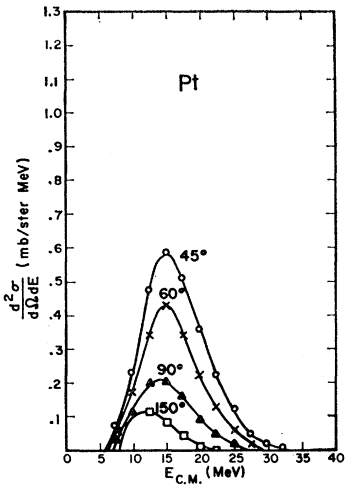

FIG. 29. Energy spectra of NCN for Pt. The identification is based on the difference between the observed and calculated spectra for compound nuclear events (see Fig. 21). Data were not collected at 30° and thus no spectrum appears for this angle.

This noncompound-nuclear group was found, as expected, to be strongly peaked in the forward direction and to be relatively most prominent at high energies. In addition, the present analysis indicates that the NCN yield dominates the high-energy part of the spectrum even at the most backward angles of observation. The NCN yields and spectral shapes (including slopes) are rather insensitive to the choice of target for targets which span a mass region from $A=58$ to $A=200$. This relative constancy of yield is in strong contrast to the marked dependence on target of the compound-nuclear yield.

ACKNOWLEDGMENTS

I wish to thank Dr. David Bodansky and Dr. Isaac Halpern for their extensive aid and helpful criticism throughout the course of this experiment and its analysis, Dr. John Blair for constructive comments, Dr. Marshall Blann for the use of his computer code, and many members of the University of Washington cyclotron staff for their aid.